

# Motion Manifold Flow Primitives for Language-Guided Trajectory Generation

Journal Title  
XX(X):1-12  
©The Author(s) 2024  
Reprints and permission:  
sagepub.co.uk/journalsPermissions.nav  
DOI: 10.1177/ToBeAssigned  
www.sagepub.com/

SAGE

Yonghyeon Lee<sup>1</sup>, Byeongho Lee<sup>2</sup>, Seungyeon Kim<sup>2</sup>, and Frank C. Park<sup>2</sup>

## Abstract

Developing text-based robot trajectory generation models is made particularly difficult by the small dataset size, high dimensionality of the trajectory space, and the inherent complexity of the text-conditional motion distribution. Recent manifold learning-based methods have partially addressed the dimensionality and dataset size issues, but struggle with the complex text-conditional distribution. In this paper we propose a text-based trajectory generation model that attempts to address all three challenges while relying on only a handful of demonstration trajectory data. Our key idea is to leverage recent flow-based models capable of capturing complex conditional distributions, not directly in the high-dimensional trajectory space, but rather in the low-dimensional latent coordinate space of the motion manifold, with deliberately designed regularization terms to ensure smoothness of motions and robustness to text variations. We show that our *Motion Manifold Flow Primitive (MMFP)* framework can accurately generate qualitatively distinct motions for a wide range of text inputs, significantly outperforming existing methods.

## Keywords

Learning from Demonstration (LfD), movement primitives, manifold learning, autoencoders, flow-based models

## Introduction

Past successes in text-based generative models for applications ranging from image synthesis (Rombach et al. 2022; Saharia et al. 2022) and 3D scene construction (Poole et al. 2022; Lin et al. 2023) to human motion generation (Zhang et al. 2022; Kim et al. 2023) can broadly be traced to two technical advancements: (i) large-scale pre-trained text embedding models based on transformer architectures (Devlin et al. 2018; Liu et al. 2019), and (ii) efficient training methods for probability density flow-based models that are capable of learning complex conditional density functions, e.g., diffusion (Ho et al. 2020; Song et al. 2020a), score-based (Song et al. 2020b), and continuous normalizing flow models (Lipman et al. 2022; Chen and Lipman 2023; Tong et al. 2023). In this paper, we address the problem of generating a set of robot motions from a user-provided text instruction.

Most existing text-based generative models rely on extensive text-annotated data for training, ranging from tens of thousands to several billion pieces of data. In contrast, we assume only a handful of demonstration data is available, making training flow-based models in high-dimensional trajectory space particularly challenging. Specifically, a flow-based model must learn a vector field that transforms the high-dimensional Gaussian distribution to the distribution of the demonstration trajectory data, as illustrated in Figure 1 (Upper). Not surprisingly, having only a small number of demonstration trajectories leads to poor generation performance, as shown later in our experiments.

Instead, leveraging a low-dimensional manifold structure can be an effective solution. Assuming the set of demonstration trajectories lies on a lower-dimensional manifold embedded in the trajectory space (the manifold

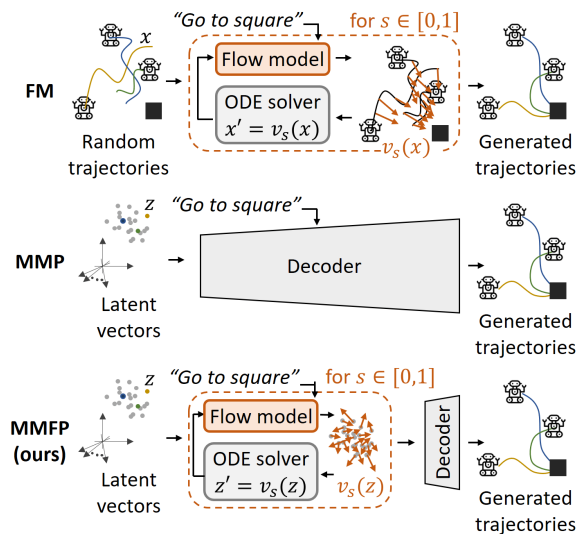


**Figure 1.** Upper: Flow-based Model (FM) in the trajectory space. Middle: Motion Manifold Primitives (MMP) with a single decoder. Lower: Motion Manifold Flow Primitives (MMFP), a flow-based model in the learned motion manifold.

hypothesis), recent works such as Motion Manifold Primitives (MMP) (Lee et al. 2023) and Task-Conditional Variational Autoencoders (TCVAE) (Noseworthy et al. 2020) exploit this structure. These methods use an autoencoder framework, where a decoder transforms a low-dimensional

<sup>1</sup> Korea Institute for Advanced Study, South Korea

<sup>2</sup> Seoul National University, South Korea

Email: ylee@kias.re.kr, yhlee.gabe@gmail.com

latent space distribution (e.g., Gaussian or Gaussian Mixture Model) to the task-conditional data distribution, given a task parameter. These models can be used by regarding texts as task parameters (Figure 1 *Middle*). However, text-conditional trajectory distributions are inherently complex, with varying numbers of modalities and volumes of support based on the input text. Our studies indicate that a single decoder network struggles to learn these complex conditional distributions.

In this paper we propose the *Motion Manifold Flow Primitive (MMFP)* framework, which combines the advantage of flow-based models capable of learning complex conditional distributions with motion manifold primitives capable of encoding and generating low-dimensional manifold of trajectories. Our proposed method consists of two steps. We first learn a decoder that parametrizes the motion manifold. In the low-dimensional latent coordinate space, we then train a flow-based model by using the recent flow matching algorithm of (Lipman et al. 2022). Specifically, to improve our model’s robustness against unseen text variations, we introduce a regularization term using the Large Language Model *ChatGPT*, significantly enhancing its robustness. As illustrated in Figure 1 (*Lower*), given a text, the latent flow-based model first transforms the low-dimensional latent Gaussian to the text-conditional latent space distribution, and then the decoder maps it to the trajectory space distribution.

We evaluate the performance of MMFP through two text-based trajectory generation tasks: (i) a bottle’s SE(3) trajectory generation for pouring task and (ii) a 7-DoF robot arm’s waving trajectory generation task. Notably, with only 10 and 30 demonstration trajectories for each respective task, MMFP shows excellent performance. In contrast, diffusion and flow-based models trained directly in the high-dimensional trajectory space (Ho et al. 2020; Lipman et al. 2022; Chen and Lipman 2023) and existing motion manifold primitives-based methods (Noseworthy et al. 2020; Lee et al. 2023) fail to generate successful trajectories.

The main contributions of our work can be summarized as follows:

- We propose MMFP that simultaneously addresses the challenges of small dataset, high-dimensionality, and complex text-dependency of trajectory distributions by integrating motion manifolds and flows, thereby achieving what neither approach can accomplish on its own;
- We propose a regularization term that leverages the recent Large Language Model *ChatGPT*, significantly improving robustness against unseen and unstructured text variations.

## Related Works

### *Movement primitives*

There are many studies on movement primitives, e.g., dynamic movement primitives (Saveriano et al. 2021; Ijspeert et al. 2013, 2001, 2002; Schaal et al. 2007; Pervez et al. 2017a; Fanger et al. 2016; Umlauf et al. 2017; Pervez et al. 2017b; Bahl et al. 2020), stable dynamical systems (Khansari-Zadeh and Billard 2011; Neumann et al. 2013; Khansari-Zadeh and Billard 2014; Lemme et al. 2014; Neumann and Steil 2015; Blocher et al. 2017; Figueroa and Billard 2018; Sindhwani et al. 2018; Kolter and Manek 2019), methods to represent diverse motions (Calinon 2016; Duque et al. 2019; Yang et al. 2018; Chernova and Veloso

2007; Paraschos et al. 2013; Noseworthy et al. 2020; Lee et al. 2023; Lee 2024). Of particular relevance to our problem is the task-conditional movement primitives. Text inputs can be transformed into text embedding vectors using pre-trained language models (Devlin et al. 2018; Liu et al. 2019), and these vectors can be treated as task parameters. Task-Parametrized Gaussian Mixture Model (TP-GMM) (Calinon 2016) is capable of generating new movements based on unseen task parameters. However, its emphasis is on a specific type of task parameters, such as frames of reference, making it unsuitable for handling text embedding vectors.

Recent deep learning methods that adopt the conditional autoencoder architectures (Noseworthy et al. 2020; Hristov and Ramamoorthy 2021; Lee et al. 2023) can take general types of task parameters and encode and generate diverse trajectories. However, as demonstrated in our later experiments, they show poor performance given the complexity of the text-conditional trajectory distributions.

### *Language-based generative models*

Recent success of text-conditional deep generative models in image (Rombach et al. 2022; Saharia et al. 2022; Ruiz et al. 2023; Zhang et al. 2023; Balaji et al. 2022), human motion (Zhang et al. 2022; Kim et al. 2023; Tevet et al. 2022), and 3D scene generation tasks (Poole et al. 2022; Lin et al. 2023) is not only attributed to transformer-based text embedding methods (Devlin et al. 2018; Liu et al. 2019; Wang et al. 2022; Li et al. 2023; Beltagy et al. 2020) and efficient training methods for flow-based conditional generative models (Ho et al. 2020; Song et al. 2020a,b; Lipman et al. 2022; Chen and Lipman 2023; Tong et al. 2023), but also relies heavily on the abundance of text-annotated training data.

In contrast, text-based generation of robot arm motions has received relatively less attention, partly due to limited demonstration data. Notable exceptions include the open X-embodiment robot learning datasets (Collaboration 2023) and generalist robotic transformers (Brohan et al. 2022), which are trained using extensive text-annotated robot motion data. However, challenges persist in generating complex 6-DoF motions, confining their capabilities primarily to simpler actions like pick-and-place. Our objective sets us apart, as we aim to develop a language-based model that can generate complex 6-DoF motions for specific tasks, yet using a limited amount of demonstration data.

## Preliminaries

### *Autoencoder-based manifold learning*

In this section, we briefly introduce an autoencoder and its manifold learning perspective (Arvanitidis et al. 2017; Lee et al. 2021, 2022a,b; Jang et al.; Lee 2023; Lee and Park 2023; Lim et al. 2024). Consider a high-dimensional data space  $\mathcal{X}$  and a set of data points  $\mathcal{D} = \{x_i \in \mathcal{X}\}_{i=1}^N$ . We adopt the manifold hypothesis that the data points  $\{x_i\}$  lie approximately on some lower-dimensional manifold  $\mathcal{M}$  in  $\mathcal{X}$ . Suppose  $\mathcal{M}$  is an  $m$ -dimensional manifold and let  $\mathcal{Z}$  be a latent space  $\mathbb{R}^m$ . An encoder is a mapping  $g : \mathcal{X} \rightarrow \mathcal{Z}$  and a decoder is a mapping  $f : \mathcal{Z} \rightarrow \mathcal{X}$ . These are often

approximated with deep neural networks and trained to minimize the reconstruction loss

$$\frac{1}{N} \sum_{i=1}^N d^2(f \circ g(x_i), x_i) \quad (1)$$

given a distance metric  $d(\cdot, \cdot)$  on  $\mathcal{X}$ . We note that, given a sufficiently low reconstruction error, all the data points  $\{x_i\}$  should lie on the image of the decoder  $f$ . Under some mild conditions – that are (i)  $m$  is lower than the dimension of the data space  $\mathcal{X}$  and (ii)  $f$  is smooth and its Jacobian  $\frac{\partial f}{\partial z}(z) \in \mathbb{R}^{\dim(\mathcal{X}) \times m}$  is full rank everywhere –, the image of  $f$  is an  $m$ -dimensional differentiable manifold embedded in  $\mathcal{X}$ , i.e., the decoder produces a lower-dimensional manifold where the data points approximately lie.

In this paper, we will treat the trajectory space as  $\mathcal{X}$  – where each element corresponds to a discrete-time trajectory – and will attempt to learn a lower-dimensional manifold of these trajectories to address the challenges of small dataset size and high dimensionality.

### Continuous normalizing flow and flow matching

In this section, we introduce the continuous normalizing flow (Chen et al. 2018) capable of fitting complex probability distributions and its efficient training method, the flow matching algorithm (Lipman et al. 2022). Let  $\{x_i \in \mathcal{X}\}_{i=1}^N$  be a set of data points sampled from the underlying probability density  $q(x)$ . Consider a non-autonomous vector field  $v : [0, 1] \times \mathcal{X} \rightarrow T\mathcal{X}$  that leads to a flow  $\phi : [0, 1] \times \mathcal{X} \rightarrow \mathcal{X}$  via the following ordinary differential equation:

$$\frac{d}{ds} \phi_s(x) = v_s(\phi_s(x)), \quad (2)$$

where  $\phi_0(x) = x$ . Given a prior density at  $s = 0$  denoted by  $p_0$ , the flow  $\phi_s$  leads to a probability density path for  $s \in [0, 1]$  (Lipman et al. 2022):

$$p_s(x) = p_0(\phi_s^{-1}(x)) \det \left( \frac{\partial \phi_s^{-1}}{\partial x}(x) \right). \quad (3)$$

Our objective is to learn a neural network model of  $v_s(x)$  so that the flow of  $v_s(x)$  transforms a simple prior density  $p_0$  (e.g., Gaussian) to the target data distribution  $p_1 \approx q$ . Then we can sample new data points by solving the ODE,  $x' = v_s(x)$ , from  $s = 0$  to  $s = 1$  with initial points sampled from  $p_0$ .

The standard maximum log-likelihood training requires expensive numerical ODE simulations (Chen et al. 2018), instead we introduce an efficient simulation-free approach for training  $v_s(x)$  (Lipman et al. 2022). In the first step, we design a conditional probability path  $p_s(x|x_1)$  for  $x_1 \sim q(x)$  such that  $p_0(x|x_1) = p_0(x)$  and  $p_1(x|x_1)$  is concentrated around  $x = x_1$ . For example, Lipman et al. (2022) suggests an Optimal Transport (OT) Gaussian probability path  $p_s(x|x_1) = \mathcal{N}(x|sx_1, (1 - (1 - \sigma_{min})s)^2 I)$  where  $\sigma_{min}$  is set to be small. Theorem 3 in (Lipman et al. 2022) states that  $u_s(x|x_1) = \frac{x_1 - (1 - \sigma_{min})x}{1 - (1 - \sigma_{min})s}$  generates the Gaussian path  $p_s(x|x_1)$ . Then, Lipman et al. (2022) shows that minimizing the following flow matching objective function

$$\mathbb{E}_{x_1 \sim q(x), s \sim \mathcal{U}[0,1], x \sim p_s(x|x_1)} [\|v_s(x) - u_s(x|x_1)\|^2], \quad (4)$$

where  $\mathcal{U}[0, 1]$  is the uniform distribution between 0 and 1, leads to a vector field  $v_s(x)$  generating  $p_1(x) = \int p_1(x|x_1)q(x_1)dx_1$  which closely approximates the data distribution  $q$ .

Our particular interest is a conditional density function  $p(x|c)$  for a condition variable  $c$  (e.g., text) which requires slight modifications. We model a neural network vector field  $v_s(x, c)$  that takes an additional input  $c$ . Then, we minimize the following objective function:

$$\mathbb{E}_{(x_1, c) \sim q(x, c), s \sim \mathcal{U}[0,1], x \sim p_s(x|x_1)} [\|v_s(x, c) - u_s(x|x_1)\|^2], \quad (5)$$

where  $q(x, c)$  is the underlying joint data distribution. In practice, sampling from  $q(x, c)$  is replaced by sampling from the dataset  $\{(x_i, c_i)\}_{i=1}^N$ .

We note that this model can represent the complex dependency of the distribution on the condition variable, e.g., when the number of modalities or the support volumes of  $p(x|c)$  vary significantly as  $c$  changes. This is because, while a single continuous neural network model is not capable of representing  $p(x|c)$  when it changes dramatically depending on  $c$ , a vector field  $v_s(x, c)$ , with an additional input  $s$ , can continuously transform the distribution as  $s$  progresses from  $s = 0$  to  $s = 1$ , thereby representing complex  $p(x|c)$ . In this work, the inherent complex text-dependency of the motion distribution will be captured by leveraging these flow-based models.

## Language-based Robot Motion Generation

We begin this section with some notations. Let  $\mathcal{Q}$  be a configuration space. Denote a sequence of configurations by  $x = (q_1, \dots, q_T)$ , called a trajectory, for  $q_i \in \mathcal{Q}$  and some positive integer  $T > 0$ . The number of configurations  $T$  is fixed throughout. We assume that the time interval between  $q_i$  and  $q_{i+1}$  is constant as  $dt$ , so the total time is  $(T - 1) \times dt$ . We will denote the trajectory space by  $\mathcal{X} = \mathcal{Q}^T$ . We use a pre-trained text encoder, the Sentence-BERT (Reimers and Gurevych 2019), without fine-tuning and it encodes free-form texts into 768-dimensional vectors; these encoded vectors are denoted by  $c$ . We assume that we are provided with a set of demonstration trajectories, each of which is annotated with  $M$  different texts, i.e., the dataset is  $\mathcal{D} = \{(x_i, \{c_{ij}\}_{j=1}^M)\}_{i=1}^N$  for  $x_i \in \mathcal{X}$  and  $c_{ij} \in \mathbb{R}^{768}$ . We will use the same symbol  $\theta$  to represent the learnable parameters of different neural networks with a slight abuse of notation, and denote a parametric neural network function by  $f_\theta(x)$  or  $f(x; \theta)$ .

The overall framework of our method is shown in Figure 2. Our framework consists of two modules: (i) the motion manifold, which addresses the challenges of small dataset size and the high dimensionality of the trajectory space  $\mathcal{Q}^T$ , and (ii) latent space flows, which are capable of capturing the complex text-dependency of the motion distribution. In the subsequent sections, we describe the training process for each module.

### Smooth Motion Manifold Learning

The motion manifold model consists of two neural networks, an encoder  $g_\theta : \mathcal{X} \rightarrow \mathcal{Z}$  and a decoder  $f_\theta : \mathcal{Z} \rightarrow \mathcal{X}$ , where  $\mathcal{Z} = \mathbb{R}^m$  is the latent space. Given a suitable distance metric

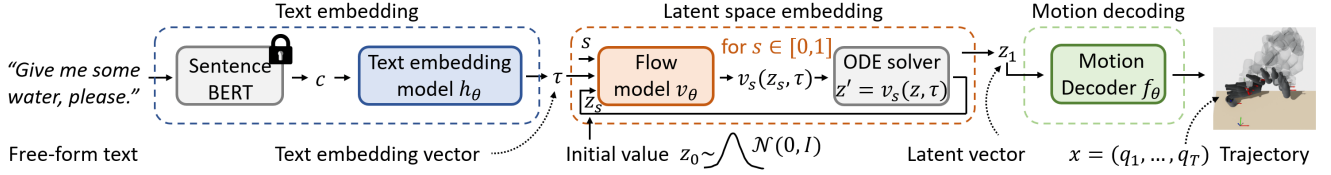


**Figure 2.** The procedure of motion generation in MMFP: (i) the Sentence-BERT encodes a free-form text into a vector  $c$ , (ii) the text embedding model  $h_\theta$  maps  $c$  to a text embedding vector  $\tau$ , (iii) we solve the ODE  $z' = v_s(z, \tau; \theta)$  from  $s = 0$  to  $s = 1$  with an initial value  $z_0$  sampled from Gaussian  $\mathcal{N}(z|0, I)$  and obtain  $z_1 \in \mathcal{Z}$ , and (iv) the motion decoder  $f_\theta$  maps  $z_1$  to a trajectory  $x = (q_1, \dots, q_T)$ .

$d(\cdot, \cdot)$  in  $\mathcal{X}$ , we train an autoencoder as follows:

$$\min_{\theta} \frac{1}{N} \sum_{i=1}^N d^2(x_i, f_\theta(g_\theta(x_i))) + \eta \|g_\theta(x_i)\|^2 + \delta \mathcal{E}(f_\theta, g_\theta), \quad (6)$$

where  $\eta, \delta$  are some positive scalars. The second term penalizes the norm of latent values to prevent them from diverging excessively far from the origin. The third term is an expected energy of the decoded trajectories, added to ensure their smoothness, which is defined as follows:

$$\mathcal{E}(f_\theta, g_\theta) := \mathbb{E}_z \left[ \frac{1}{T-1} \sum_{t=1}^{T-1} \left\| \frac{f_\theta^{t+1}(z) - f_\theta^t(z)}{dt} \right\|^2 \right], \quad (7)$$

where  $f_\theta(z) = (f_\theta^1(z), \dots, f_\theta^T(z)) \in \mathcal{Q}^T$ . The latent value  $z$  in this expectation is sampled with augmentation as  $z = \alpha g_\theta(x_i) + (1 - \alpha) g_\theta(x_j)$ , where  $\alpha \sim \mathcal{U}[-0.4, 1.4]$  and  $x_i, x_j$  are sampled from the dataset, to extend the regularization effect to regions where data is not available, adopting (Lee et al. 2022b). We have empirically observed that with sufficiently low-dimensional latent spaces and smooth activation functions, the decoder  $f_\theta$  satisfies the injective immersion condition, and the trained decoder parametrizes an  $m$ -dimensional motion manifold embedded in the trajectory space (see the preliminary section on manifold learning).

### Robust Text-conditional Latent Flow Learning

The latent space flow-based model consists of two neural networks. One is a text embedding neural network  $h_\theta$  that maps  $c \mapsto \tau = h_\theta(c) \in \mathcal{T}$ , where  $\mathcal{T} = \mathbb{R}^p$  is called a text embedding space. The other is a neural network vector field  $v(\cdot; \theta)$  in the latent space that maps  $(s, z, \tau) \mapsto v_s(z, \tau; \theta) \in T_z \mathcal{Z}$ , where  $T_z \mathcal{Z}$  is the tangent space of  $\mathcal{Z}$  at  $z$ . We train these two networks simultaneously with the following *regularized* flow matching loss:

$$\min_{\theta} \frac{1}{NM} \sum_{i=1}^N \sum_{j=1}^M \left( \mathbb{E}_{s, z} [\|v_s(z, h_\theta(c_{ij}); \theta) - u_s(z|z_i)\|^2] + \frac{\gamma}{K} \sum_{k=1}^K \|h_\theta(c_{ij}) - h_\theta(\tilde{c}_{ij}^k)\|^2 \right). \quad (8)$$

In the expectation of the first term,  $s, z$  are sampled from  $\mathcal{U}[0, 1]$ ,  $p_s(z|z_i)$ , respectively, and  $p_s(z|z_i)$  is defined as the OT Gaussian path and  $u_s(z|z_i)$  is derived from it (see the preliminary section on flow matching). The second term, multiplied by a positive weight  $\gamma$ , is added to ensure robustness against diverse text variations. Here,  $\tilde{c}_{ij}^k$  are Sentence-BERT encoding vectors that have meanings similar to those of  $c_{ij}$ , which are generated via the Large Language Model *ChatGPT*.

Using the trained text embedding model  $h_\theta$ , vector field  $v_\theta$ , and decoder  $f_\theta$ , we can generate, given a free-form text input, diverse trajectories by the following procedure (see Figure 2): (i) encode the text input using the Sentence-BERT to  $c$ , (ii) embed  $c$  to a text embedding vector  $\tau = h_\theta(c)$ , (iii) solve an ODE  $z' = v_s(z, \tau; \theta)$  from  $s = 0$  to  $s = 1$  with initial samples  $z_0 \sim p_0(z) = \mathcal{N}(z|0, I)$  and obtain  $z_1 \in \mathcal{Z}$  – where we use Euler method with  $ds = 0.05$  –, and (iv) map the ODE solutions  $z_1$  to trajectories  $x = f_\theta(z_1)$ . We call this framework *Motion Manifold Flow Primitives (MMFP)*.

We note that our MMFP, which solves the ODE in the latent space to obtain a single latent value and maps it to the entire trajectory  $z \mapsto x = (q_1, \dots, q_T)$ , fundamentally differs from conventional latent ODE methods that model and map the latent trajectory  $(z_1, \dots, z_T)$  to the trajectory  $x = (q_1, \dots, q_T)$  (Rubanova et al. 2019; Zhi et al. 2022).

Lastly, one may ask a reasonable question: Why not use diffusion models (Song et al. 2020b) in the latent space instead of flow models, which are known for their ability to fit complex conditional distributions? We note that flow-based models trained via flow matching – rather than the conventional maximum likelihood method – can be understood as deterministic versions of diffusion models (Lipman et al. 2022). In our trajectory generation tasks, empirical results show that latent flow models outperform diffusion models (see the experiment section on the comparison of latent diffusion and flow models). This performance gap is likely due to the relatively small size of our trajectory dataset.

## Experiments

In this section, we evaluate our method, the MMFP, mainly compared to (i) Denoising Diffusion Probabilistic Models (DDPM) (Ho et al. 2020) trained in the trajectory space  $\mathcal{X}$  – when  $\mathcal{X}$  is  $\text{SE}(3)^T$ , we train DDPM in local coordinates –, (ii) Flow Matching (FM) (Lipman et al. 2022) trained in the trajectory space  $\mathcal{X}$  – when  $\mathcal{X}$  is  $\text{SE}(3)^T$ , we use the Riemannian Flow Matching (RFM) (Chen and Lipman 2023) –, (iii) Task-Conditional Variational Autoencoder (TCVAE) with Gaussian prior (Noseworthy et al. 2020), and (iv) Motion Manifold Primitives with Gaussian mixture prior (MMP) (Lee et al. 2023). MMFP trained without the regularization term (i.e., the second term in (8)) in the latent flow learning will be denoted by MMFP w/o reg.

For MMFP, we choose the latent space dimension  $m = 3$  for  $\mathcal{Z} = \mathbb{R}^m$  and text embedding dimension  $p = 3$  for  $\mathcal{T} = \mathbb{R}^p$ . For TCVAE and MMP, with thorough tuning, we set the latent space dimension to be 3 or 4 and text embedding dimension to be 64. We compare models for 6-DoF  $\text{SE}(3)$  pouring trajectory generation and 7-DoF

robot arm waving motion generation tasks. Throughout, we use fully-connected neural networks with ELU activation functions.

**Evaluation metrics:** The primary objective is to generate correct motions corresponding to the given text inputs. To evaluate whether the model generates accurate motions that perform the task described in the given text, we train a trajectory classifier and use it to report the motion accuracy; the higher, the better. Additionally, the model should be able to generate not just a single trajectory but diverse trajectories, imitated from the given demonstration dataset, depending on the text input. For example, see Figure 6 and 12. We use the Maximum Mean Discrepancy (MMD) (Gretton et al. 2012) – which measures the distance between two probability distributions, computed from their samples – to measure the similarity between the set of generated trajectories given a text input and the set of demonstration trajectories annotated with that text; the lower, the better. A formal mathematical expression of the MMD metric is provided below: let  $\{x_i\}_{i=1}^N$  and  $\{y_j\}_{j=1}^M$  be the samples of  $p(x)$  and  $p(y)$  in the metric space  $\mathcal{X}$  with a distance metric denoted by  $d_{\mathcal{X}}(\cdot, \cdot)$ . First, we define a symmetric positive kernel  $k(x, y) := \exp(-\frac{d_{\mathcal{X}}^2(x, y)}{h})$ , where  $h := \sum_{i,j=1}^{N+M} \frac{d_{\mathcal{X}}^2(z_i, z_j)}{(N+M)(N+M-1)}$  for  $z_i \in \{x_1, \dots, x_N, y_1, \dots, y_M\}$ . Then the MMD metric  $\text{MMD}(p(x), p(y))$  is computed as

$$\frac{1}{N^2} \sum_{i,j=1}^N k(x_i, x_j) + \frac{1}{M^2} \sum_{i,j=1}^M k(y_i, y_j) - \frac{2}{NM} \sum_{i=1}^N \sum_{j=1}^M k(x_i, y_j). \quad (9)$$

Texts are annotated to each trajectory at multiple different levels (e.g., see Figure 5 Left and Figure 10), and the MMD metrics are measured separately for each level text input, then averaged across text descriptions at the same level. Evaluation metrics are computed using both seen and unseen texts in training. First, accuracy and MMD metrics are measured using the seen texts. Then, to evaluate the robustness to text variations, we also report robust MMD metrics, which are computed with unseen unbiased text inputs generated by ChatGPT.

We begin this section by comparing latent diffusion and flow models using two-dimensional collision-free trajectory generation tasks. Additionally, we present experiments with higher-dimensional configuration spaces, the text-based SE(3) pouring motion generation and 7-DoF waving motion generation tasks.

### Comparison of Latent Diffusion and Flow Models with 2D Trajectory Generation

In this section, we provide deeper insights into latent flow matching algorithms by comparing flows trained with the Optimal Transport (OT) path and various diffusion-based paths. Recall that we first train a motion manifold of trajectories, followed by training a flow model in the latent coordinate space. The flow matching algorithm includes a key design choice: selecting the conditional probability paths  $p_s(x|x_1)$  (see the preliminary section on the flow matching). This section investigates how different path choices affect the outcomes. For illustration purposes, we use a simple example: a text-based 2D trajectory generation task.

Lipman et al. (2022) demonstrated that flow matching in certain cases can recover diffusion processes. Diffusion

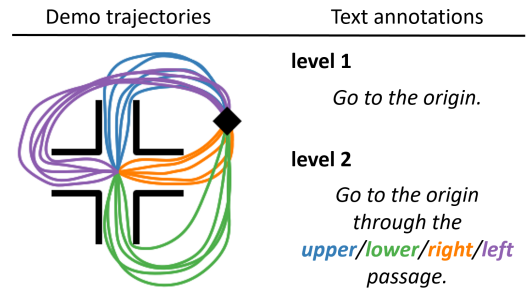


**Figure 3.** Demonstration trajectories with multiple text annotations. Each trajectory is assigned with two text labels, the level 1 and level 2 texts.

**Table 1.** MMFPs trained with OT and various diffusion paths. The same motion manifold (i.e., an autoencoder) is employed.

	MMD ( $\downarrow$ )		Accuracy ( $\uparrow$ )	
	level 1	level 2	path	task
Diffusion-VE	0.075	0.007	100	94.6
Diffusion-VP-1	0.073	<b>0.003</b>	100	95.0
Diffusion-VP-2	0.030	0.055	94.3	81.0
Optimal Transport	<b>0.025</b>	<b>0.004</b>	<b>100</b>	<b>99.8</b>

models (Song et al. 2020a; Ho et al. 2020) gradually corrupt data by adding noise, which leads the data to approach pure noise over time. These processes can be represented as Gaussian conditional probability paths,  $p_s(x|x_1) = \mathcal{N}(x|\mu_s(x_1), \sigma_s^2(x_1)I)$ , where the forward diffusion process corresponds to  $s = 1 \rightarrow s = 0$ . Specific choices of mean  $\mu_s(x_1)$  and variance  $\sigma_s(x_1)$  determine the nature of the path.

For example, Variance Exploding (VE) path has the form

$$p_s(x|x_1) = \mathcal{N}(x|x_1, \sigma_{1-s}^2 I), \quad (10)$$

where  $\sigma_s$  is an increasing function,  $\sigma_0 = 0$  and  $\sigma_1 \gg 1$ . The Variance Preserving (VP) diffusion paths has the form

$$p_s(x|x_1) = \mathcal{N}(x|\alpha_{1-s}x_1, (1 - \alpha_{1-s}^2)I), \quad (11)$$

where  $\alpha_s = \exp(-\frac{1}{2}T(s))$ ,  $T(s) = \int_0^s \beta(s')ds'$ , and  $\beta(s')$  is the noise scale function.

Lipman et al. (2022) also showed that these diffusion paths align with the vector fields used in deterministic probability flow for score-based models (Song et al. 2020b). Compared to diffusion paths, they found that the OT Gaussian path results in smoother ODE trajectories. This makes it easier for neural network vector fields to fit the data, improving accuracy and reducing the number of function evaluations required during sampling.

We reproduce and reinterpret these findings – originally obtained with image datasets – using our own 2D trajectory dataset with text annotations (shown in Figure 3) and extend them with a novel interpretation in the context of MMFP. In our dataset, there are 20 demonstration trajectories that do not collide with the wall, all starting from the same point and ending at a common goal point (the origin). There are four distinct passages to the origin, with five trajectories passing through each passage (upper, lower, right, and left). Each trajectory has a length of  $T = 201$ , and the trajectory space is  $\mathcal{X} = \mathbb{R}^{2T}$ . For each trajectory  $x_i \in \mathcal{X}$ , we assign two text annotations: level 1 (the same for all trajectories, “Go to the origin”) and level 2 (providing more specific instructions, shared among groups of five trajectories).

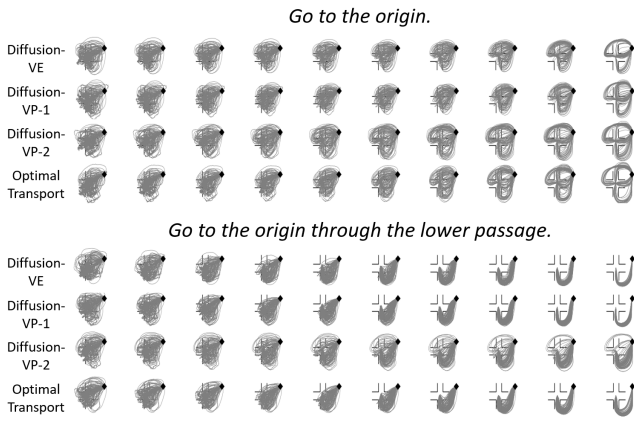


**Figure 4.** Evolution of generated trajectories (from left to right) follows each of the latent vector fields trained with different Gaussian paths, including both diffusion paths and the Optimal Transport path, with the trajectories on the far right representing the final output samples.

We use the same motion manifold (an autoencoder) and train latent vector fields with different Gaussian probability paths: variance exploding path with  $\sigma_{1-s} = 3(1-s)$  denoted by Diffusion-VE, variance preserving paths with  $\alpha_{1-s} = e^{-5(1-s)^2}$  denoted by Diffusion-VP-1 and  $\alpha_{1-s} = e^{-0.5(1-s)^2}$  denoted by Diffusion-VP-2, and the optimal transport path.

Table 1 shows Diffusion-VE, Diffusion-VP-1, Diffusion-VP-2, and Optimal Transport, the last of which is utilized in our MMFP throughout the paper. We note that Optimal Transport path consistently yields the best results. Figure 4 illustrates the evolution of generated trajectories following each of the latent vector fields, described by  $z'_s = v_s(z_s, \tau)$ , where at each  $z_s$  is mapped to a 2D trajectory through the decoder function. The trajectories displayed on the far right represent the final output samples. Optimal Transport is shown to provide the best outcomes.

Unlike image-based generative models trained with large datasets, the limited data in our case amplifies the impact of the chosen probability path. While in image models the primary advantage of using the Optimal Transport path is faster sampling, here it improves generative performance by learning a model with a smoother velocity field, which proves to be crucial for generalization with small trajectory datasets. Therefore, the latent flow models of our MMFP presented in the subsequent section are always trained with Optimal Transport paths.

### Text-based pouring motion generation

In this section, we train text-based pouring motion generation models, where the dataset is obtained from the human demonstration videos. The demonstrator is instructed to pour water or wine in five different pouring directions (i.e., from the very left, left, center, right, and very right side). When pouring wine, the demonstrator is instructed to turn the wrist clockwise at the end. From ten videos, we extract SE(3) trajectories of the bottles, and the trajectory lengths are pre-processed so that  $T = 480$ . For each trajectory  $x_i \in \mathcal{X}$ , we give three text annotations, i.e.,  $\{c_{ij}\}_{j=1}^M$  for  $M = 3$  as shown in Figure 5 (Left).

Table 2 shows MMD, robust MMD, and Accuracy; our MMFP only shows good scores in all metrics. We note that the regularization in MMFP significantly improves the level 3 robust MMD metric. The DDPM and RFM overall produce very poor MMD results. As shown in Figure 5 (Right), the trajectory generated by DDPM does not even converge near the cup and that of RFM is very jerky. TCVAE and MMP, both adopting the motion manifold hypothesis, produce motions of reasonable quality. Nevertheless, they exhibit a limitation in understanding level 3 text descriptions, particularly regarding pouring directions. Examples illustrating this limitation can be observed in Figure 5 (Right), where they fail in pouring from accurate directions. Lastly, Figure 6 shows a variety of accurately generated motions by MMFP given unbiased user text inputs not seen during training.

To understand why TCVAE and MMP fail, it’s essential to understand the conditional AutoEncoder (cAE) architecture. In a cAE, the decoder takes a latent value and a text embedding vector together as inputs to generate a trajectory as the output. However, the single decoder network in a cAE struggles to fit a complex, non-smooth function like the one in this example, where the text-conditional trajectory distribution changes dramatically across level 1, 2, and 3 texts. On the other hand, our latent flow-based models can capture such complex distributions because they smoothly transform the distributions not all at once but gradually via the ODE.

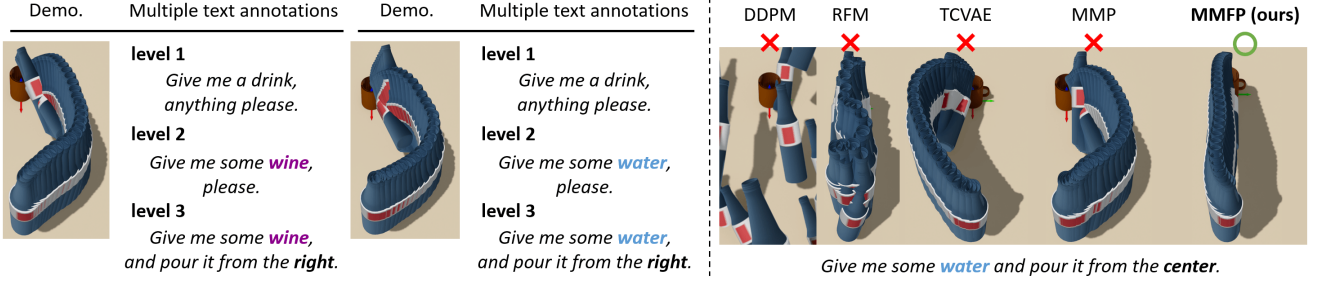
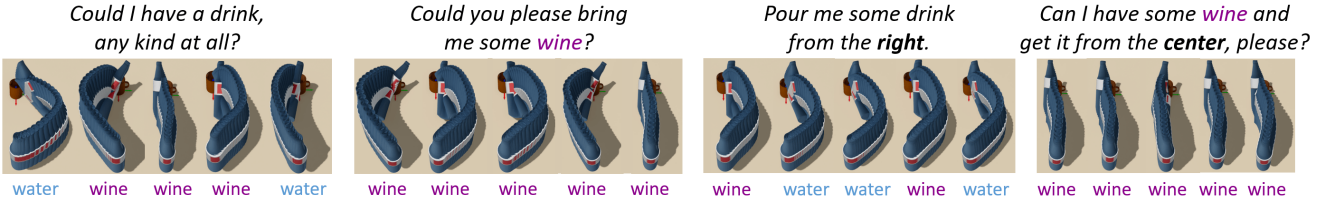
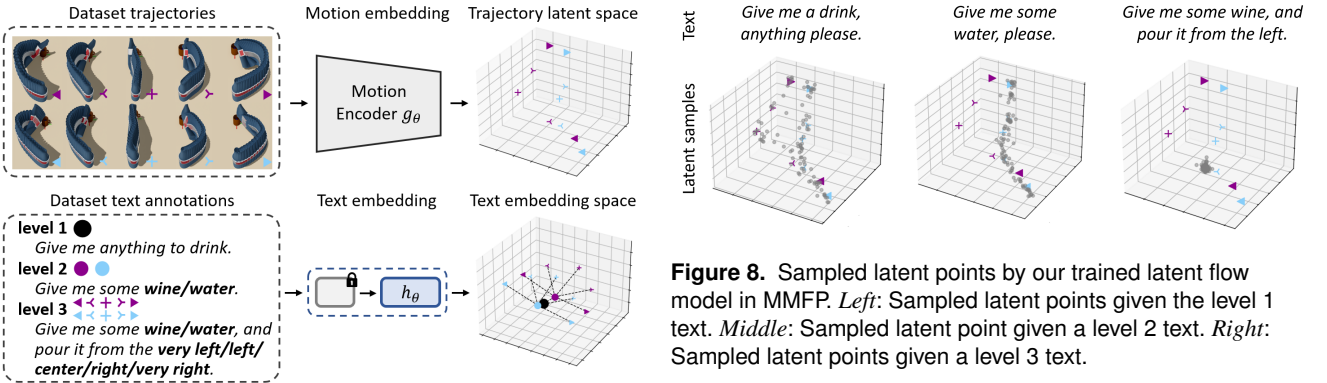
We provide a visual analysis of the latent distributions of the SE(3) pouring dataset in our MMFP. Trajectory data themselves are very high-dimensional and hence difficult to visualize. Fortunately, since our motion manifold models use three-dimensional latent spaces, the distributions of the data in the latent space can be visualized. Additionally, the text embedding space also has a dimension of three, so text embedding vectors can be visualized as well. Figure 7 shows the latent distributions of both the trajectory data and the text embeddings.

Figure 8 highlights the multi-modality of the text-conditioned latent distribution and, more importantly, the dramatic change in the distribution as the text inputs vary. In the figure, moving from left to right corresponds to scenarios where level 1 to level 3 texts are given as inputs. When a level 1 text is provided, the distribution must fit two modalities, and the volume of the distribution is the largest. In contrast, when level 2 or level 3 texts are provided, there is only one modality. Note that the support of the distribution varies significantly from level 1 to level 3, becoming much smaller at level 3. This implies that a latent text-conditioned distribution should capture such dramatic changes, fitting a complex, non-smooth function. Conditional autoencoder models struggle to fit such a complex function, while our latent flow models are capable of doing so.

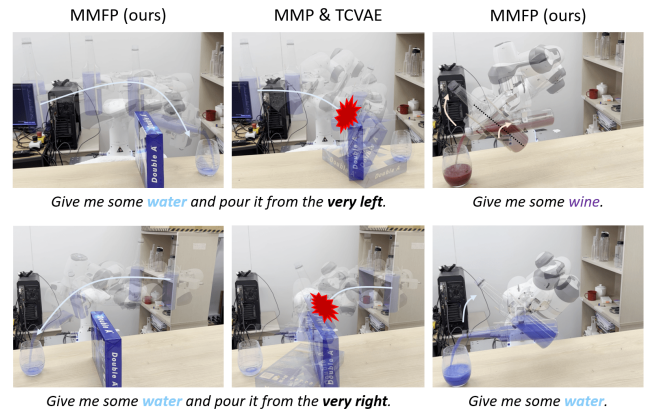
We conduct real robot experiments with two scenarios. First, we put an obstacle blocking the middle path, and ask the robot “Give me some water, and pour it from the very left/right side.”, so that it pours water while turning away to avoid collision, without relying on vision systems but by correctly understanding human instructions; see Figure 9 (Upper). Second, we ask the robot “Give me some wine/water.”, and see if it shows clockwise rotation behavior

**Table 2.** The MMD and robust MMD metrics and the accuracy (%) for pouring motion generation.

	MMD ( $\downarrow$ )			robust MMD ( $\downarrow$ )			Accuracy ( $\uparrow$ )		
	level 1	level 2	level 3	level 1	level 2	level 3	pouring style	pouring direction	both
DDPM (Ho et al. 2020)	0.398	0.484	1.306	0.400	0.486	1.304	50.5	20.0	10.2
RFM (Chen and Lipman 2023)	0.411	0.431	0.778	0.413	0.425	1.127	87.0	36.4	30.8
TCVAE (Noseworthy et al. 2020)	0.117	0.211	0.824	0.131	0.191	1.041	52.0	25.4	15.3
MMP (Lee et al. 2023)	<b>0.045</b>	<b>0.115</b>	0.950	<b>0.055</b>	<b>0.112</b>	0.970	47.5	19.6	9.3
MMFP w/o reg (ours)	<b>0.055</b>	<b>0.114</b>	<b>0.009</b>	<b>0.056</b>	<b>0.097</b>	0.096	<b>98.5</b>	<b>93.2</b>	<b>99.9</b>
MMFP (ours)	<b>0.042</b>	<b>0.093</b>	<b>0.007</b>	<b>0.052</b>	<b>0.094</b>	<b>0.016</b>	<b>99.0</b>	<b>92.6</b>	<b>99.9</b>

**Figure 5.** Left: Example demonstration trajectories, each of which is annotated with three different level texts. Right: Generated pouring trajectories by RFM, TCVAE, MMP and MMFP.**Figure 6.** A variety of accurate trajectories generated by MMFP given unbiased text inputs.**Figure 7.** Upper: SE(3) pouring trajectory data encoded in the three-dimensional latent space by our motion encoder  $g_\theta$ . Lower: Texts used in training encoded in the three-dimensional text embedding space by our text embedding model  $h_\theta$ .**Table 3.** Real robot success rates given language guidance.

	TCVAE	MMP	MMFP (ours)
EXP 1 (very left side)	0/3	1/3	3/3
EXP 2 (very right side)	0/3	2/3	3/3
EXP 3 (wine)	1/3	1/3	2/3
EXP 4 (water)	0/3	1/3	3/3

**Figure 8.** Sampled latent points by our trained latent flow model in MMFP. Left: Sampled latent points given the level 1 text. Middle: Sampled latent point given a level 2 text. Right: Sampled latent points given a level 3 text.**Figure 9.** Real robot pouring motion generation results.

of the bottle at the end of the pouring; see Figure 9 (Lower). Given generated SE(3) trajectories of the bottle, we compute joint space trajectories by solving the inverse kinematics. Since this process can be computationally intensive, we train and use a neural IK classifier for fast and feasible joint trajectory computation; details can be found in Appendix A. We generate three joint space trajectories for each text input, and measure the success rates. Success is judged by human observation. Table 3 shows the success rates (trajectories from DDPM and RFM are not implemented because they are too jerky to be deployed in the real robot). MMFP outperforms TCVAE and MMP in all experiments. We note that, in EXP 3, the success rate of MMFP is 2/3. Judging by human observation, one trajectory is somewhat ambiguous to determine whether the robot is pouring water or pouring wine. Figure 9 shows examples where MMFP successfully understands human instructions, thereby avoiding the obstacle and demonstrating the correct pouring style.

Regarding the obstacle avoidance experiments, one may ask, what if it is difficult for the user to instruct the avoidance direction? We note that if a vision system capable of recognizing obstacles and performing collision checking is available, then our framework can indeed be equipped with an autonomous obstacle avoidance mechanism. This can be achieved by searching for a proper latent value that leads to a collision-free trajectory, i.e., finding one that is collision-free within the motion manifold. Specifically, given multiple latent samples, we can use a decoder function  $f_\theta$  to map them to trajectories, and then check whether the trajectories are collision-free. If the obstacle blocks the trajectory pouring from the center, trajectories that avoid it by pouring from the left or right will be sampled. However, if there are very strict constraints, such as multiple obstacles blocking all paths, a solution may not exist. Intuitively, learning a larger motion manifold that contains a greater diversity of motions increases the likelihood of finding a solution. Therefore, ensuring diversity in the demonstration data, which limits the diversity of the motion manifold, although costly, is crucial for improving the adaptability of the system.

### Text-based 7-DoF waving motion generation

In this section, we train text-based 7-DoF waving motion generation models, where the dataset is obtained from human demonstrations. The demonstrator is instructed to hold and move the robot arm so that the robot arm mimics waving motions in five different viewing directions (i.e., very left, left, front, right, and very right) and in three different styles (i.e., very big, big, small). We extract 7-DoF joint space trajectories, and the trajectory lengths are pre-processed to ensure  $T = 720$ . Thus,  $\mathcal{Q} = \mathbb{R}^7$ , and the trajectory space is denoted as  $\mathcal{X} = \mathbb{R}^{7 \times T}$ . We encode two motions for each setting, resulting in a total of  $N = 30$  trajectories. For each trajectory  $x_i \in \mathcal{X}$ , we provide three text annotations, denoted by  $\{c_{ij}\}_{j=1}^M$  for  $M = 3$ , as shown in Figure 10. Thus, multiple trajectories can be associated with a single text label; for example, all 30 trajectories are labeled with the level 1 text, ‘Wave your hand.’ In the following, we compare our MMFP with the FM, TCVAE and MMP, both quantitatively and qualitatively.

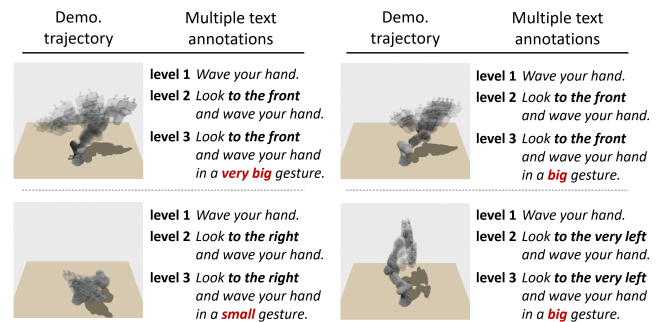


**Figure 10.** Example 7-DoF demonstration trajectories, each of which is assigned with three different text labels.

Table 4 shows MMD, robust MMD, and Accuracy; MMFP again only shows good scores in all metrics. We also note that the regularization in MMFP significantly improves the level 3 robust MMD metric. The DDPM and FM again produce very poor MMD results, and their generated trajectories generated, as shown in Figure 11, are very jerky. TCVAE and MMP, both adopting the motion manifold hypothesis, produce motions of reasonable quality. Nevertheless, they exhibit a limitation in understanding detailed text instructions, both level 2 and level 3. Examples illustrating this limitation can be observed in Figure 11, where they fail in waving to accurate directions and with accurate styles. Lastly, Figure 12 shows a variety of accurately generated motions by MMFP, given unbiased user text inputs not seen during training. Some real robot waving motion generation results by our MMFP are visualized in Figure 13.

## Conclusion

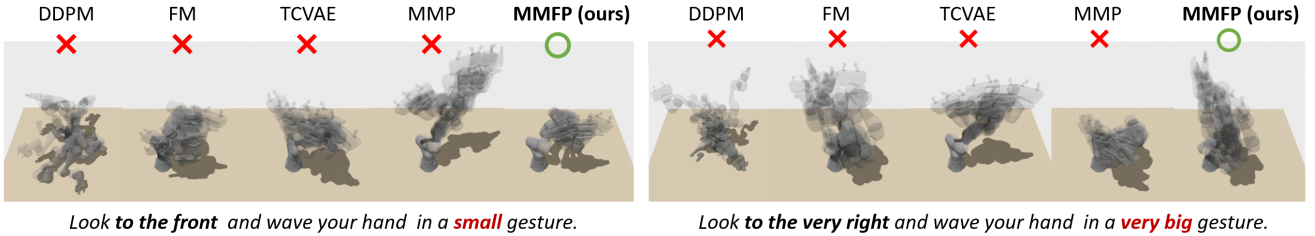
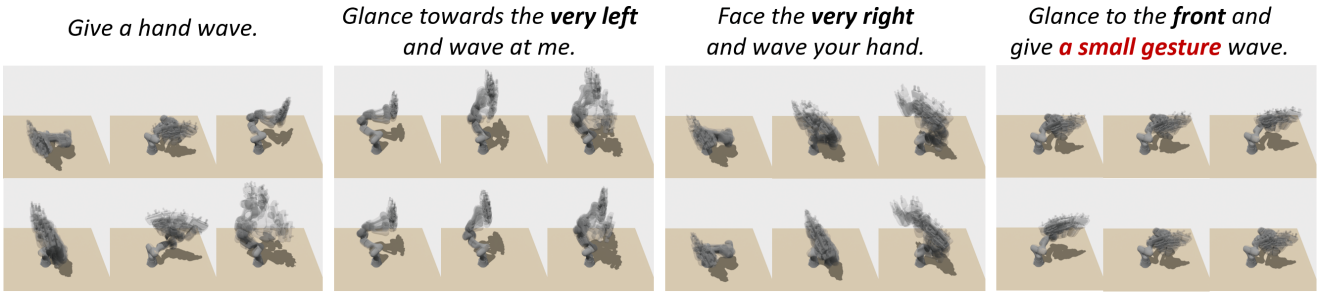
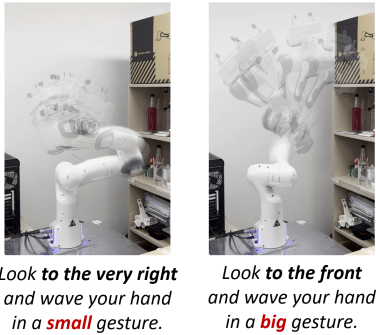
The Motion Manifold Flow Primitive (MMFP) framework combines motion manifolds and latent flows, enabling models to learn complex text-conditional distributions with dramatic changes in the number of modalities and support volumes based on text inputs, all while relying on a small number of trajectory data, each labeled with multiple text annotations. Proper regularization has been designed to ensure the smoothness of the generated trajectories and robustness to unstructured text variations. The performance of the MMFP framework has been validated through extensive experiments involving the generation of SE(3) and 7-DoF joint trajectories. Our results demonstrate accurate motion generation even for unseen text inputs generated by the Large Language Model, ChatGPT. This contrasts with existing manifold-based methods, such as TCVAE and MMP, which struggle with text inputs containing detailed descriptions, and trajectory space diffusion and flow-based models, which tend to produce jerky trajectories.

We believe the MMFP framework can be enhanced in several ways. The current implementation only uses text as input to the model. To develop more versatile movement primitives, incorporating visual inputs as an additional conditional vector will be crucial. For example, in a pouring task, the trajectory should depend on the type of bottle, whether it’s a kettle, a can, etc., with the bottle’s geometry provided as a depth image or point cloud. Developing models conditioned on both text and visual inputs may require



**Table 4.** The MMD and robust MMD metrics and the accuracy (%) for waving motion generation.

	MMD ( $\downarrow$ )			robust MMD ( $\downarrow$ )			Accuracy ( $\uparrow$ )		
	level 1	level 2	level 3	level 1	level 2	level 3	waving direction	waving style	both
DDPM (Ho et al. 2020)	0.425	0.542	0.831	0.427	0.542	0.831	18.4	29.3	4.1
FM (Lipman et al. 2022)	0.211	0.368	0.646	0.215	0.384	0.671	<b>99.6</b>	88.7	91.1
TCVAE (Noseworthy et al. 2020)	0.269	0.581	0.833	0.294	0.606	0.865	25.6	57.3	10.7
MMP (Lee et al. 2023)	<b>0.013</b>	0.369	0.772	<b>0.016</b>	0.355	0.750	19.2	30.7	6.5
MMFP w/o reg (ours)	<b>0.020</b>	<b>0.037</b>	<b>0.006</b>	<b>0.024</b>	<b>0.046</b>	<b>0.021</b>	<b>99.8</b>	<b>98.7</b>	<b>99.7</b>
MMFP (ours)	<b>0.016</b>	<b>0.040</b>	<b>0.004</b>	<b>0.022</b>	<b>0.040</b>	<b>0.005</b>	<b>100</b>	<b>97.7</b>	<b>100</b>

**Figure 11.** Generated waving trajectories by DDPM, FM, TCVAE, MMP and MMFP.**Figure 12.** A variety of accurate trajectories generated by MMFP given unbiased text inputs.**Figure 13.** Real robot waving motion generation by MMFP.

more sophisticated neural network architectures to learn generalizable primitives from small datasets, which presents a challenging yet important problem.

Adopting a more structured text embedding space could enhance text generalization performance compared to the current vector space approach. Poincaré embeddings, known for effectively learning hierarchical representations (Nickel and Kiela 2017), have shown promise in this regard. Given the hierarchical nature of text descriptions – such as the level 1, 2, and 3 texts discussed in our paper – hyperbolic embeddings can be particularly well-suited for capturing these relationships. Incorporating this type of structured geometry into our framework offers an intriguing direction for future research.

Our current framework relies on fixed-length discrete-time trajectory data, and thus demonstration trajectories must be pre-processed to have the same length. This requirement could potentially be relaxed by using sequence models, such as transformers or recurrent neural networks, which can handle variable-length data, for the decoder model, whereas the current implementation uses fully connected neural networks. Alternatively, as recently presented in (Lee 2024), using continuous-time representations with parametric curve models is another promising direction.

## Acknowledgements

Yonghyeon Lee was the beneficiary of an individual grant from CAINS supported by a KIAS Individual Grant (AP092701) via the Center for AI and Natural Sciences at Korea Institute for Advanced Study. Byeongho Lee, Seungyeon Kim, and Frank C. Park were supported in part by IITP-MSIT grant RS-2021-II212068 (SNU AI Innovation Hub), IITP-MSIT grant RS-2022-II220480 (Training and Inference Methods for Goal Oriented AI Agents), IITP-MSIT grant RS-2024-00436680 (Collaborative Research Projects with Microsoft Research), KIAT grant P0020536 (HRD Program for Industrial Innovation), ATC+ MOTIE Technology Innovation Program grant 20008547, SRRC NRF grant RS-2023-00208052, SNU-AIIS, SNU-IPAI, SNU-IAMD, SNU BK21+ Program in Mechanical Engineering, and SNU Institute for Engineering Research.

## References

- Arvanitidis G, Hansen LK and Hauberg S (2017) Latent space oddity: on the curvature of deep generative models. *arXiv preprint arXiv:1710.11379*.
- Bahl S, Mukadam M, Gupta A and Pathak D (2020) Neural dynamic policies for end-to-end sensorimotor learning. *Advances in Neural Information Processing Systems* 33: 5058–5069.
- Balaji Y, Nah S, Huang X, Vahdat A, Song J, Kreis K, Aittala M, Aila T, Laine S, Catanzaro B, Karras T and Liu MY (2022) ediffi: Text-to-image diffusion models with an ensemble of expert denoisers. *arXiv preprint arXiv:2211.01324*.
- Beltagy I, Peters ME and Cohan A (2020) Longformer: The long-document transformer. *arXiv:2004.05150*.
- Blocher C, Saveriano M and Lee D (2017) Learning stable dynamical systems using contraction theory. In: *2017 14th International Conference on Ubiquitous Robots and Ambient Intelligence (URAI)*. IEEE, pp. 124–129.
- Brohan A, Brown N, Carbajal J, Chebotar Y, Dabis J, Finn C, Gopalakrishnan K, Hausman K, Herzog A, Hsu J, Ibarz J, Ichter B, Irpan A, Jackson T, Jesmonth S, Joshi NJ, Julian R, Kalashnikov D, Kuang Y, Leal I, Lee KH, Levine S, Lu Y, Malla U, Manjunath D, Mordatch I, Nachum O, Parada C, Peralta J, Perez E, Pertsch K, Quiambao J, Rao K, Ryoo M, Salazar G, Sanketi P, Sayed K, Singh J, Sontakke S, Stone A, Tan C, Tran H, Vanhoucke V, Vega S, Vuong Q, Xia F, Xiao T, Xu P, Xu S, Yu T and Zitkovich B (2022) Rt-1: Robotics transformer for real-world control at scale. *arXiv preprint arXiv:2212.06817*.
- Calinon S (2016) A tutorial on task-parameterized movement learning and retrieval. *Intelligent service robotics* 9: 1–29.
- Chen RT and Lipman Y (2023) Riemannian flow matching on general geometries. *arXiv preprint arXiv:2302.03660*.
- Chen RT, Rubanova Y, Bettencourt J and Duvenaud DK (2018) Neural ordinary differential equations. *Advances in neural information processing systems* 31.
- Chernova S and Veloso M (2007) Confidence-based policy learning from demonstration using gaussian mixture models. In: *Proceedings of the 6th international joint conference on Autonomous agents and multiagent systems*. pp. 1–8.
- Collaboration OXE (2023) Open x-embodiment: Robotic learning datasets and rt-x models. *arXiv preprint arXiv:2310.08864*.
- Devlin J, Chang MW, Lee K and Toutanova K (2018) Bert: Pre-training of deep bidirectional transformers for language understanding. *arXiv preprint arXiv:1810.04805*.
- Duque DA, Prieto FA and Hoyos JG (2019) Trajectory generation for robotic assembly operations using learning by demonstration. *Robotics and Computer-Integrated Manufacturing* 57: 292–302.
- Fanger Y, Umlauf J and Hirche S (2016) Gaussian processes for dynamic movement primitives with application in knowledge-based cooperation. In: *2016 IEEE/RSJ International Conference on Intelligent Robots and Systems (IROS)*. IEEE, pp. 3913–3919.
- Figuroa N and Billard A (2018) A physically-consistent bayesian non-parametric mixture model for dynamical system learning. In: *CoRL*. pp. 927–946.
- Gretton A, Borgwardt KM, Rasch MJ, Schölkopf B and Smola A (2012) A kernel two-sample test. *The Journal of Machine Learning Research* 13(1): 723–773.
- Ho J, Jain A and Abbeel P (2020) Denoising diffusion probabilistic models. *Advances in neural information processing systems* 33: 6840–6851.
- Hristov Y and Ramamoorthy S (2021) Learning from demonstration with weakly supervised disentanglement. In: *Ninth International Conference on Learning Representations 2021*.
- Ijspeert AJ, Nakanishi J, Hoffmann H, Pastor P and Schaal S (2013) Dynamical movement primitives: learning attractor models for motor behaviors. *Neural computation* 25(2): 328–373.
- Ijspeert AJ, Nakanishi J and Schaal S (2001) Trajectory formation for imitation with nonlinear dynamical systems. In: *Proceedings 2001 IEEE/RSJ International Conference on Intelligent Robots and Systems. Expanding the Societal Role of Robotics in the the Next Millennium (Cat. No. 01CH37180)*, volume 2. IEEE, pp. 752–757.
- Ijspeert AJ, Nakanishi J and Schaal S (2002) Learning rhythmic movements by demonstration using nonlinear oscillators. In: *Proceedings of the IEEE/RSJ int. conference on intelligent robots and systems (iros2002)*, CONF. pp. 958–963.
- Jang C, Lee Y, Noh YK and Park FC (????) Geometrically regularized autoencoders for non-euclidean data. In: *The Eleventh International Conference on Learning Representations*.
- Khansari-Zadeh SM and Billard A (2011) Learning stable nonlinear dynamical systems with gaussian mixture models. *IEEE Transactions on Robotics* 27(5): 943–957.
- Khansari-Zadeh SM and Billard A (2014) Learning control lyapunov function to ensure stability of dynamical system-based robot reaching motions. *Robotics and Autonomous Systems* 62(6): 752–765.
- Kim J, Kim J and Choi S (2023) Flame: Free-form language-based motion synthesis & editing. In: *Proceedings of the AAAI Conference on Artificial Intelligence*, volume 37. pp. 8255–8263.
- Kolter JZ and Manek G (2019) Learning stable deep dynamics models. *Advances in neural information processing systems* 32.
- Lee B, Lee Y, Kim S, Son M and Park FC (2023) Equivariant motion manifold primitives. In: *Conference on Robot Learning*. PMLR, pp. 1199–1221.
- Lee Y (2023) A geometric perspective on autoencoders. *arXiv preprint arXiv:2309.08247*.
- Lee Y (2024) Mmp++: Motion manifold primitives with parametric curve models. *IEEE Transactions on Robotics*.
- Lee Y, Kim S, Choi J and Park F (2022a) A statistical manifold framework for point cloud data. In: *International Conference on Machine Learning*. PMLR, pp. 12378–12402.
- Lee Y, Kwon H and Park F (2021) Neighborhood reconstructing autoencoders. *Advances in Neural Information Processing Systems* 34: 536–546.
- Lee Y and Park FC (2023) On explicit curvature regularization in deep generative models. In: *Topological, Algebraic and Geometric Learning Workshops 2023*. PMLR, pp. 505–518.
- Lee Y, Yoon S, Son M and Park FC (2022b) Regularized autoencoders for isometric representation learning. In: *International Conference on Learning Representations*.
- Lemme A, Neumann K, Reinhart RF and Steil JJ (2014) Neural learning of vector fields for encoding stable dynamical systems. *Neurocomputing* 141: 3–14.

- Li Z, Zhang X, Zhang Y, Long D, Xie P and Zhang M (2023) Towards general text embeddings with multi-stage contrastive learning.
- Lim J, Kim J, Lee Y, Jang C and Park FC (2024) Graph geometry-preserving autoencoders. In: *Forty-first International Conference on Machine Learning*.
- Lin CH, Gao J, Tang L, Takikawa T, Zeng X, Huang X, Kreis K, Fidler S, Liu MY and Lin TY (2023) Magic3d: High-resolution text-to-3d content creation. In: *Proceedings of the IEEE/CVF Conference on Computer Vision and Pattern Recognition*. pp. 300–309.
- Lipman Y, Chen RT, Ben-Hamu H, Nickel M and Le M (2022) Flow matching for generative modeling. *arXiv preprint arXiv:2210.02747*.
- Liu Y, Ott M, Goyal N, Du J, Joshi M, Chen D, Levy O, Lewis M, Zettlemoyer L and Stoyanov V (2019) Roberta: A robustly optimized bert pretraining approach. *arXiv preprint arXiv:1907.11692*.
- Neumann K, Lemme A and Steil JJ (2013) Neural learning of stable dynamical systems based on data-driven lyapunov candidates. In: *2013 IEEE/RSJ International Conference on Intelligent Robots and Systems*. IEEE, pp. 1216–1222.
- Neumann K and Steil JJ (2015) Learning robot motions with stable dynamical systems under diffeomorphic transformations. *Robotics and Autonomous Systems* 70: 1–15.
- Nickel M and Kiela D (2017) Poincaré embeddings for learning hierarchical representations. *Advances in neural information processing systems* 30.
- Noseworthy M, Paul R, Roy S, Park D and Roy N (2020) Task-conditioned variational autoencoders for learning movement primitives. In: *Conference on robot learning*. PMLR, pp. 933–944.
- Paraschos A, Daniel C, Peters JR and Neumann G (2013) Probabilistic movement primitives. *Advances in neural information processing systems* 26.
- Pervez A, Ali A, Ryu JH and Lee D (2017a) Novel learning from demonstration approach for repetitive teleoperation tasks. In: *2017 IEEE World Haptics Conference (WHC)*. IEEE, pp. 60–65.
- Pervez A, Mao Y and Lee D (2017b) Learning deep movement primitives using convolutional neural networks. In: *2017 IEEE-RAS 17th international conference on humanoid robotics (Humanoids)*. IEEE, pp. 191–197.
- Poole B, Jain A, Barron JT and Mildenhall B (2022) Dream-fusion: Text-to-3d using 2d diffusion. *arXiv preprint arXiv:2209.14988*.
- Reimers N and Gurevych I (2019) Sentence-bert: Sentence embeddings using siamese bert-networks. In: *Proceedings of the 2019 Conference on Empirical Methods in Natural Language Processing*. Association for Computational Linguistics. URL <https://arxiv.org/abs/1908.10084>.
- Rombach R, Blattmann A, Lorenz D, Esser P and Ommer B (2022) High-resolution image synthesis with latent diffusion models. In: *Proceedings of the IEEE/CVF conference on computer vision and pattern recognition*. pp. 10684–10695.
- Rubanova Y, Chen RT and Duvenaud DK (2019) Latent ordinary differential equations for irregularly-sampled time series. *Advances in neural information processing systems* 32.
- Ruiz N, Li Y, Jampani V, Pritch Y, Rubinstein M and Aberman K (2023) Dreambooth: Fine tuning text-to-image diffusion models for subject-driven generation. In: *Proceedings of the IEEE/CVF Conference on Computer Vision and Pattern Recognition*. pp. 22500–22510.
- Saharia C, Chan W, Saxena S, Li L, Whang J, Denton EL, Ghasemipour K, Gontijo Lopes R, Karagol Ayan B, Salimans T, Ho J, J Fleet D and Norouzi M (2022) Photorealistic text-to-image diffusion models with deep language understanding. *Advances in Neural Information Processing Systems* 35: 36479–36494.
- Saveriano M, Abu-Dakka FJ, Kramberger A and Peternel L (2021) Dynamic movement primitives in robotics: A tutorial survey. *arXiv preprint arXiv:2102.03861*.
- Schaal S, Mohajerian P and Ijspeert A (2007) Dynamics systems vs. optimal control—a unifying view. *Progress in brain research* 165: 425–445.
- Sindhwani V, Tu S and Khansari M (2018) Learning contracting vector fields for stable imitation learning. *arXiv preprint arXiv:1804.04878*.
- Song J, Meng C and Ermon S (2020a) Denoising diffusion implicit models. *arXiv preprint arXiv:2010.02502*.
- Song Y, Sohl-Dickstein J, Kingma DP, Kumar A, Ermon S and Poole B (2020b) Score-based generative modeling through stochastic differential equations. *arXiv preprint arXiv:2011.13456*.
- Tevet G, Raab S, Gordon B, Shafir Y, Cohen-Or D and Bermano AH (2022) Human motion diffusion model. *arXiv preprint arXiv:2209.14916*.
- Tong A, Malkin N, Hugué G, Zhang Y, Rector-Brooks J, Fatras K, Wolf G and Bengio Y (2023) Conditional flow matching: Simulation-free dynamic optimal transport. *arXiv preprint arXiv:2302.00482*.
- Umlauf J, Fanger Y and Hirche S (2017) Bayesian uncertainty modeling for programming by demonstration. In: *2017 IEEE International Conference on Robotics and Automation (ICRA)*. IEEE, pp. 6428–6434.
- Wang L, Yang N, Huang X, Jiao B, Yang L, Jiang D, Majumder R and Wei F (2022) Text embeddings by weakly-supervised contrastive pre-training. *arXiv preprint arXiv:2212.03533*.
- Yang C, Chen C, Wang N, Ju Z, Fu J and Wang M (2018) Biologically inspired motion modeling and neural control for robot learning from demonstrations. *IEEE Transactions on Cognitive and Developmental Systems* 11(2): 281–291.
- Zhang C, Zhang C, Zhang M and Kweon IS (2023) Text-to-image diffusion model in generative ai: A survey. *arXiv preprint arXiv:2303.07909*.
- Zhang M, Cai Z, Pan L, Hong F, Guo X, Yang L and Liu Z (2022) Motiondiffuse: Text-driven human motion generation with diffusion model. *arXiv preprint arXiv:2208.15001*.
- Zhi W, Lai T, Ott L, Bonilla EV and Ramos F (2022) Learning efficient and robust ordinary differential equations via invertible neural networks. In: *International Conference on Machine Learning*. PMLR, pp. 27060–27074.

## Appendix A: Fast Inverse Kinematics with Neural IK Classifier

It is often useful to train motion generative models in the object configuration space  $\mathcal{Q}$  (e.g.,  $SE(3)$  for a rigid body object) rather than in the joint space of a robot arm. In this

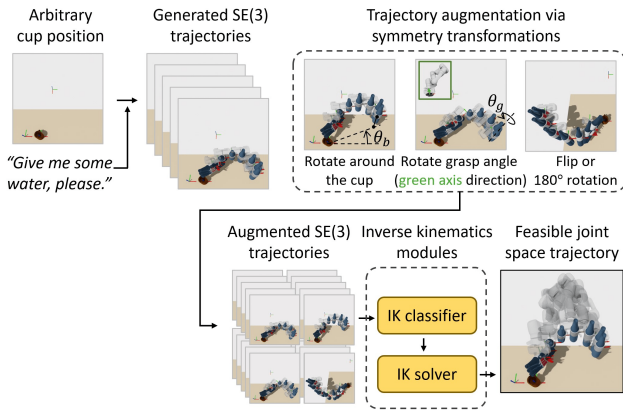


**Figure 14.** The procedure of a feasible joint space trajectory generation.

way, the trained generative models can be used without being constrained by (i) the specific relative position of an object to the robot base, (ii) the type of robot, and (iii) the end-effector or tool in use.

In this scenario, we need to determine a robot joint space trajectory that produces the given trajectory of an object. For example, suppose we have a SE(3) water-pouring trajectory of a bottle. We first need to determine where to grasp, i.e., the end-effector’s relative pose with respect to the bottle frame, and then need to solve the Inverse Kinematics (IK) to find out the corresponding joint space motion. Depending on the bottle’s trajectory and grasping pose, an IK solution may or may not exist.

Hence, it is often necessary to iterate multiple times, generating an object’s motion and verifying the existence of an IK solution. While motion generative models can quickly generate multiple motions, the IK solver demands a comparatively substantial amount of time. Therefore, there is a practical need for a method that can quickly determine the feasibility of target object trajectories, given a robot’s kinematic structure. In this work, we propose to train a *Neural Inverse Kinematics (Neural IK) classifier* that can predict the feasibility of target object trajectories very fast in parallel. The neural IK classifier is used to narrow down the candidate SE(3) trajectories to which we need to apply the numerical IK, thereby significantly reduces the overall computation time.

Using the neural IK classifier, we propose a method to quickly find feasible joint space trajectories for an arbitrary 2D position of the cup when provided with SE(3) trajectories of a bottle sampled using our MMFP; see Figure 14 for the overview. To begin, for a given SE(3) trajectory of a bottle, we leverage symmetries in the pouring task to augment it into diverse SE(3) trajectories. This augmentation involves three types of transformations, as illustrated in Figure 14 (Trajectory augmentation via symmetry transformations): (1) rotation of the bottle around the cup axis by  $\theta_b \in [-30^\circ, 30^\circ]$ , (2) rotation of the bottle frame by  $\theta_g \in [-60^\circ, 60^\circ]$  that changes the grasping pose – where the robot reaches and grasps the bottle in the green axis direction –, and (3) flipping the bottle with respect to the cup (i.e., rotating it by  $180^\circ$ ). Each generated trajectory undergoes a total of  $50 = 5 \times 5 \times 2$  transformations. This involves

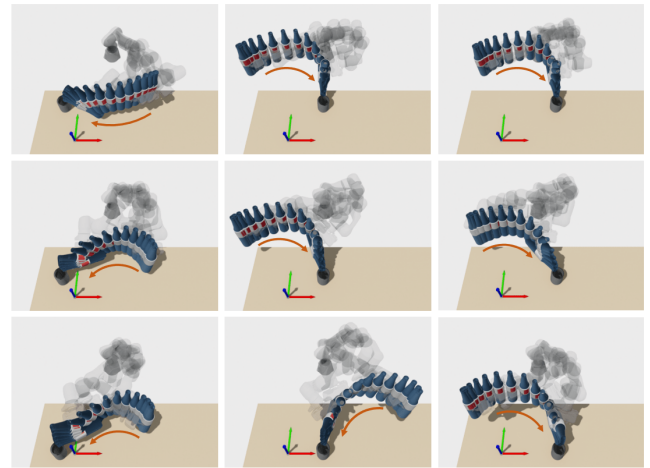


**Figure 15.** Various IK solutions given diverse configurations of the cup.

discretizing  $[-30^\circ, 30^\circ]$  and  $[-60^\circ, 60^\circ]$  into 5 points with equal-size intervals for  $\theta_b$  and  $\theta_g$ , respectively. Additionally, multiples of 2 are considered for flipping. We generate five trajectories for a single text input, resulting in a total of 250 candidate SE(3) trajectories that require verification for the existence of an IK solution.

Our neural IK classifier, applied to 250 trajectories in parallel, demonstrates remarkably fast speeds in predicting IK feasibility, taking on average 0.0157 seconds with a CPU and 0.0002 seconds with a GPU. We train the neural IK classifier with 18000 training trajectory data and evaluate the classification accuracy on 9000 unseen test trajectory data. The test set accuracy is 98.14%. While the 1.86% classification error may raise concerns, it is not a critical issue, because our plan is to narrow down the candidate SE(3) trajectories using the classifier and apply the numerical IK for the reduced set of candidate trajectories anyway. Example SE(3) trajectories whose IK solution exist are shown in Figure 15.